

SCIENTIFIC REPORTS



OPEN

Establishing the limits of efficiency of perovskite solar cells from first principles modeling

Oscar Grånäs^{1,2}, Dmitry Vinichenko³ & Efthimios Kaxiras^{1,4}

Received: 22 July 2016

Accepted: 10 October 2016

Published: 08 November 2016

The recent surge in research on metal-halide-perovskite solar cells has led to a seven-fold increase of efficiency, from ~3% in early devices to over 22% in research prototypes. Oft-cited reasons for this increase are: (i) a carrier diffusion length reaching hundreds of microns; (ii) a low exciton binding energy; and (iii) a high optical absorption coefficient. These hybrid organic-inorganic materials span a large chemical space with the perovskite structure. Here, using first-principles calculations and thermodynamic modelling, we establish that, given the range of band-gaps of the metal-halide-perovskites, the theoretical maximum efficiency limit is in the range of ~25–27%. Our conclusions are based on the effect of level alignment between the perovskite absorber layer and carrier-transporting materials on the performance of the solar cell as a whole. Our results provide a useful framework for experimental searches toward more efficient devices.

Photovoltaic applications of metal halide perovskite absorbers face a number of outstanding challenges, including materials stability, hysteresis effects of the current-voltage characteristics, and fine-tuning of the absorption properties^{1,2}. The perovskite ABX₃ structure, where A and B are typically organic or inorganic cations, and X is an oxygen or halogen anion, offers a large chemical phase space, allowing many properties to be tailored, albeit not independently. We argue that reaching the ideal efficiency, apart from optimizing the quality of materials and interfaces, is more challenging than optimizing the photo absorber; when absorption properties are tailored by adjusting the composition, band alignment and effective masses are also affected.

To establish the theoretical limits of efficiency, we assume ideal interfaces and defect-free crystals. We investigate how the presence of different ions on the A, B and X site of the perovskite structure impacts the photovoltaic performance, using electronic structure calculations and available experimental information, together with thermodynamic considerations. We show that the level alignment to the electron- and hole-transporting media (ETM and HTM) is central to reaching maximum efficiency for heterogeneous positive-intrinsic-negative (PIN) junctions. In fact, the efficiency limit for many of the perovskites is similar, in the ~25–27% range, given perfect band-alignment to ETM and HTM. Current state-of-the-art cells reach >80% of the theoretical maximum efficiency, indicating that higher performance is mostly a matter of interface engineering and the construction of multi-junction cells. Our results shed light into the performance differences arising from different perovskite compositions, choices of electron and hole transporting media or modification of the heterojunctions^{3,4}. Thus, they serve as a guide to further work on what HTM and ETM are suitable for optimal device performance.

Model of the solar cell

We aim to establish theoretical limits for the power conversion efficiency (PCE) of the perovskite-based solar cells as a function of chemical composition of the perovskite layer and the electronic properties of the electron- and hole-transporting media, by using the thermodynamic approach pioneered by Shockley and Queisser⁵. Recent experiments indicate that exotic effects such as ferroelectricity are not responsible for the reported high efficiencies^{6,7}. The most important properties of the perovskites as photo-absorbers are the resilience to form recombination centres and the reasonable interface quality to many ETMs and HTMs. Thus, it is reasonable to determine efficiency limits of perovskite solar cells from arguments based on detailed balance. Experimental

¹John A. Paulson School of Engineering and Applied Sciences, Harvard University, Cambridge, Massachusetts 02138, United States. ²Department of Physics and Astronomy, Division of Materials Theory, Uppsala University, Box 516, SE-75120 Uppsala, Sweden. ³Department of Chemistry and Chemical Biology, Harvard University, Cambridge, Massachusetts 02138, United States. ⁴Department of Physics, Harvard University, Cambridge, Massachusetts 02138, United States. Correspondence and requests for materials should be addressed to O.G. (email: oscar.granas@physics.uu.se)

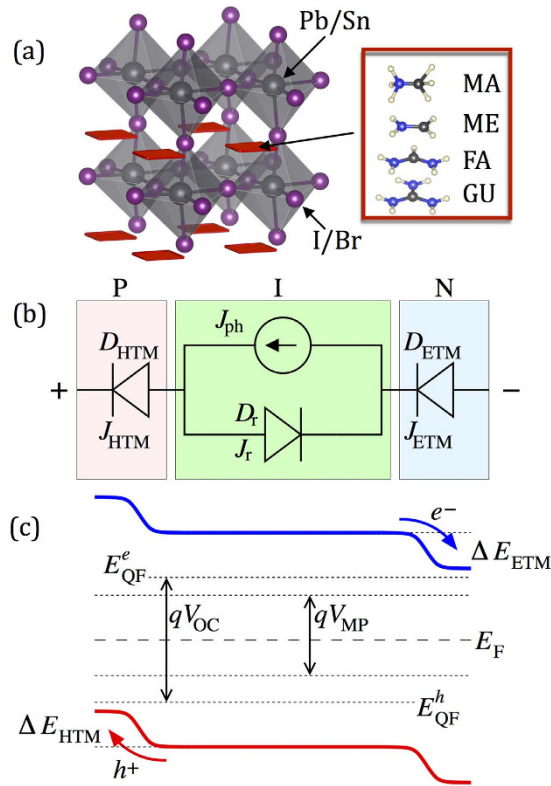


Figure 1. (a) Composition of perovskites under consideration (in the organic cation, blue = N, black = C, white = H). (b) Equivalent circuit of the PIN photoabsorbing heterostructure. J_{ph} denotes the photon induced current, D_r the intrinsic diode (additional diode currents from Shockley-Reed-Hall recombination can be added), $D_{ETM/HTM}$ represent rectifying diodes, the diode voltage drop, as well as forward direction is determined by the energy level alignment. (c) Schematic overview of the energy level diagram of the intrinsic part, with band offsets ΔE_{HTM} , ΔE_{HTM} to ETM/HTM. E_F is the position of the Fermi level, E_{QF}^h , E_{QF}^e the quasi Fermi-levels under illumination with open circuit, V_{MP} the voltage for the maximum power point and V_{oc} the open-circuit voltage.

characterization of the heterojunctions suggests that perovskite solar cells are of PIN character^{8,9}, where the perovskite itself comprises the central intrinsic semiconductor. We model the cell as a PIN heterojunction, where the carriers are generated by photon absorption in the intrinsic perovskite layer, separated and injected across a corresponding interface into the electron- or hole-transporting medium. We model interfaces between the perovskite and carrier transporting media as diodes $D_{ETM/HTM}$ with the constant voltage drop (CVD) approximation, that is, we ignore the band matching character. We also ignore back transfer of carriers, which has been experimentally proven a slow process¹⁰. We present in Fig. 1(b) a schematic of the circuit. We assume a constant-entropy mode of operation; with that, the electrochemical potential of the cell can be expressed as:

$$\Delta\mu = eV_{ext} = E_G - k_B T \ln \left[\frac{2\pi k_B T}{h^2} \frac{4(m_e^* m_h^*)^{3/2}}{n_e n_h} \right] - \Delta E_{HTM} - \Delta E_{ETM}, \tag{1}$$

where E_G is the perovskite absorber band gap, m_e^* , m_h^* are carrier effective masses, n_e , n_h are carrier densities, and ΔE_{HTM} , ΔE_{ETM} are the potential drops at the boundaries between the perovskite layer and carrier-transporting media. The energy levels in our model are shown in Fig. 1(c). We ignore shunt and series resistances, and consider only radiative recombination to provide the upper limit for experimental efforts. With these assumptions, the current is given by $J = e(N_{ph} - RR(V_{ext}))$, where N_{ph} is the density of absorbed photons, and $RR(V_{ext})$ is the rate of radiative recombination:

$$RR(V_{ext}) = e \frac{2\pi}{c^2 h^3} \exp(eV_{ext}/k_B T) \int_{E_G}^{\infty} \frac{E^2 dE}{\exp(E/k_B T) - 1} \tag{2}$$

In order to compute the PCE, we use the NREL reference AM1.5 spectrum normalized to 1 kW/m². The maximal extractable power density is determined by maximizing $P = V_{ext} \cdot J(V_{ext})$. From these considerations, we can identify three main components that determine the efficiency of the perovskite-based solar cell: the band gap of the absorber, the carrier characteristics relevant for entropic contribution, and the alignment between absorber

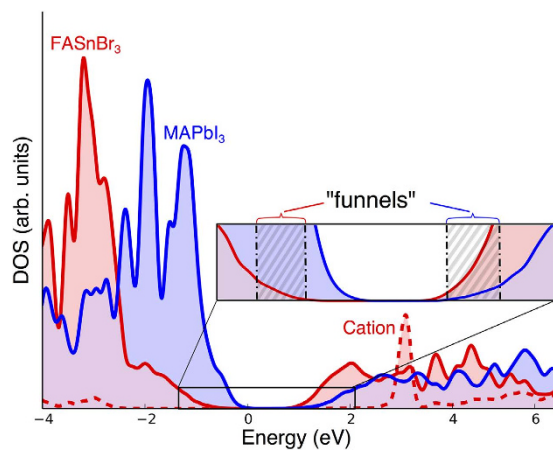


Figure 2. Densities of states for methylammonium lead iodide (MAPbI₃) and formamidinium tin bromide (FASnBr₃), showing contributions from the organic cation and the inorganic sublattice. The band edges are spanned by metal and halogen states, with the cation having only minor hybridization. The inset shows the shallow DOS ('funnel') near the VBM, characteristic for tin-based compounds, and shallow DOS near the CBM, typical of Pb-based compounds (see text for details).

and carrier transporting media. In the following we discuss our approach to determining these quantities using a combination of first-principles modelling and available experimental data.

The band gap of the perovskites is generally direct, or close to direct¹¹. Together with band edge characters that allow for dipolar transitions this leads to an extraordinarily high optical absorption coefficient, which allows for a thin-film cell architecture. The onset of absorption is determined by the band gap, which is crucial for estimating the fraction of absorbed photon flux.

In the context of first-principles electronic structure calculations with density functional theory (DFT), due to incorrect Coulomb interaction asymptotes in semi-local functionals¹², the band gap is underestimated; for the hybrid organic-inorganic perovskites the error between different DFT calculations is fairly constant (for instance, the difference between the gaps of MASnI₃ and MAPbI₃ is only 0.07 eV, as inferred by comparison with GW results)^{13–15}. In order to obtain realistic band gaps for the compounds studied here, we use MAPbI₃ (for which reliable experimental data is available) as the reference material and calculate the difference in the DFT computed gap with all other compounds. We employ two different methods for calculating the shifts in band gap of the perovskites under consideration, the results range between 1.2 eV and 2.1 eV (in PBE) or between 0.9 eV and 2.3 eV (in HSE).

Experimentally, the photo-induced excitons dissociate rapidly into free carriers due to low exciton binding energy of 10–50 meV^{16,17}; for this reason it is not necessary to model excitonic effects.

Charge mobility is a very important factor for efficient solar cells and is key to the high reported efficiencies. Long mean free paths have been observed in experiments: early work measured over 1 μm for polycrystalline samples⁹ while more recent work reported values up to 175 μm under illumination and 3 mm under weak light¹⁸. Apart from the diffusion length, the low carrier masses decrease the entropic loss of the open-circuit voltage. Small masses are manifested as funnel-like structures on the electronic density of states, with a minimal number of states at the band edges¹⁹. The perovskite compounds have a pronounced funnel effect (see Fig. 2), which contributes to the high cell efficiency at operating temperatures. We compute the average of the effective mass tensor of the carriers from the band structure using a high density (approximately 2×10^7 k-points/ \AA^{-3}) mesh. Finally, we determine the entropy contribution of the excited carriers to the quasi Fermi level splitting using an effective density of excited states of 10^{15} cm^{-3} . The carrier masses of the compounds under consideration are smaller than, for example, Si which results in a smaller effect of the temperature arising from carrier entropy and a smaller deviation from the Shockley-Queisser limit²⁰. The results show a clear trend: Pb compounds have lower conduction band mass and higher valence band mass in relation to the Sn counterparts. The effective masses range between 0.1 and 0.3 in units of m_e .

Properties like the natural level alignment and the absorption onset are difficult to measure from an experimental point of view²¹. Interface and surface dipoles, defects and sample inhomogeneities result in substantial differences in available experimental data. For example, the depletion layer is reported to be somewhere between 45 to 300 nm^{22,23}, indicating that level alignments play a crucial role for the carrier concentrations and for the potential gradient in the perovskite. The calculation of the natural band alignment from first principles using core levels or by inspecting how the average electrostatic potential changes on a site in different environments has been treated extensively in the literature^{24,25}. We employ a method of alignment similar to what was first suggested by Massidda *et al.*²⁶, and later refined by Wei and Zunger²⁷, and by Lang *et al.*²⁸. We estimate the relative positions of valence and conduction bands of perovskites with different composition using the average electrostatic potential on the B site ion, or, in the case of B-ion substitution, on the X-site ion. We also use the equivalent formalism of core-levels as a test for consistency. The band alignments, from the relative position of band edges to those of MAPbI₃, are used to map the corresponding potential drops for the rectifying diodes appearing at

the heterojunctions between the perovskite and the charge-transporting media. We do not explicitly model the P and N materials; instead, we map out the efficiency as a function of the natural band alignment with respect to MAPbI₃. Recent computational work provided estimates for the potential alignment of a number of common semiconductors in relation to MAPbI₃; with our results, this can be used directly to estimate how the efficiency is altered²⁹.

MAPbI₃ has a cubic structure at high temperature and undergoes a transition to a tetragonal structure close to room temperature. The two phases are known to co-exist to much lower temperatures. To reduce the complexity of calculating the level alignments, we concentrate on the cubic phase of the perovskite cell. This involves calculating: the core-level (CL) alignment in the super cell between the left (L) and right (R) perovskites; the CL alignment to valence band maxima (VBM) in the *strained* materials (with strain according to the relaxed heterostructure); the CL alignment to VBM in the relaxed structure. To account for possible steric effects from the orientation of the organic cations, we consider them oriented in the plane orthogonal to the super cell stacking, which resembles the tetragonal phase. This procedure allows us to determine the natural band alignment between MAPbI₃ and the other perovskites under consideration. Results for all compounds are available in the Supplementary Material. Reviewing other theoretical approaches reveals a significant spread in reported data^{30,31}, but the trends are consistent with our findings. Previous work on GaAs/AlAs heterojunctions estimated errors in absolute value on the order of 0.05 eV²⁶. For the calculations reported here, we expect slightly larger errors due to the complex symmetry breaking by the organic cation. Previous studies using similar methods but without taking into account strain effects reported similar values of band alignment for the compounds under consideration³².

In cases where an increase (decrease) in the potential for electrons (holes) occurs, the voltage drop over the junction depends exponentially on the barrier height, with most of the external bias over the junction. In these cases, the quasi Fermi-level splitting goes to zero, inducing strong recombination in the junction, and the value of J_{sc} effectively goes to zero as well. An accurate treatment of the junctions requires knowledge of the dielectric properties and density of states of specific HTMs and ETMs.

Results and Discussion

We have investigated 16 hybrid organic-inorganic compounds with the perovskite structure of the general composition ABX₃. For A, we have considered 4 organic cations, the traditionally used methylammonium, and three other ions of similar size and conjugated π system of increasing size: methyleneiminium (ME = CH₂NH₂⁺), formamidinium (FA = CH(NH₂)₂⁺) and guanidinium (GU = C(NH₂)₃⁺). We consider Pb²⁺ and Sn²⁺ ions for the B position, and Cl⁻ and Br⁻ ions for the X position. The most important feature of the electronic structure of these compounds is that, regardless of the size of the π system of the A cation, the band edges are spanned by *s*- and *p*-states of the B ion and by *p*-states of the X ion. The A ions act mostly as spacers and affect the electronic structure and properties of the perovskite through the changes they induce in lattice structure, as we discuss below.

The bottom of the conduction band is spanned mostly by the *p*-states of B ions with an admixture of *p*-states of X-ions. There are two factors in action when the B site is changed: the relative electronegativity of Pb and Sn, and the strength of spin-orbit coupling, which leads to splitting of the bottom of the conduction band. Those factors lead to lowering of the absolute position of the CBM for Sn compared to Pb. Moreover, due to stronger spin-orbit coupling in Pb, the CBM splitting is larger, which leads to higher curvature of the CBM and, therefore, to lower effective masses for electrons in Pb-based perovskites (~0.1 m_e) compared to Sn-based perovskites (~0.2–0.3 m_e). With Br in the X position the CBM is higher due to the more covalent character of the bonds and larger splitting between bonding and antibonding orbitals.

The top of the valence band consists of an antibonding combination of X *p*-states and B *s*-states leading to a lower absolute position of the VBM with increasing electronegativity of the X ion. Substitution of Pb by Sn on the B site leads to an increase of the VBM energy due to larger overlap of the Sn *s*-states with the X *p*-orbitals. An increase in the size of the A cation leads to a decrease in the VBM energy due to expansion of the lattice structure from the decrease in overlap between the *s*-orbitals of B and the *p*-orbitals of X, and the concomitant lowering of the antibonding level energy. Smaller overlap between the *s*-orbitals of B and the *p*-orbitals of X also leads to a less dispersive band and an increase in the effective carrier mass for the holes for Pb (~0.15–0.3 m_e) compared to Sn (~0.07–0.1 m_e). A similar effect is introduced by increasing the size of the A cation. Another factor is the Darwin term effect on the *s*-orbitals of B ion levels, which is larger for Pb, resulting in flatter bands.

From the absolute positions of the CBM and VBM we obtain the value of the band gap, which is in the 1.1–1.6 eV range for most compounds except for FA-, MA-, and GU-based perovskites with PbBr₃ lattice backbone. Based on our calculations, we conclude that all of the compounds studied (except for those mentioned above) demonstrate power conversion efficiency of 25–27% regardless of actual chemical composition, provided optimal band alignment is satisfied. This clearly demonstrates that the intrinsic properties of hybrid organic-inorganic compounds, that is, band gap and carrier effective masses, are not the limiting factor in determining the efficiency. Rather, it is the misalignment of the absolute positions of the band edges that can lead to substantial performance deterioration (about 5% PCE for every 0.2 eV of mismatch, see Supplementary Material Fig. 3). We map out the band edge positions, which are equivalent to the optimal carrier-transporting material levels, and the PCE achieved with optimal level matching in Fig. 3. Our overall conclusion is that experimental efforts should be directed towards optimization of the device as a whole, using as a guide the results outlined above.

In particular, the chemical composition of the perovskite has a profound effect on the position of VBM and CBM levels: an increase in the size of the A ion leads to lowering of the VBM; compounds with Pb on the B site have lower VBM and higher CBM compared to Sn-based perovskites; Br-based compounds have lower VBM and higher CBM compared to I-based ones. These principles can be used to tailor the composition of the perovskite absorber in order to optimize the efficiency of the cell overall by ensuring optimal level matching with the carrier-transporting materials.

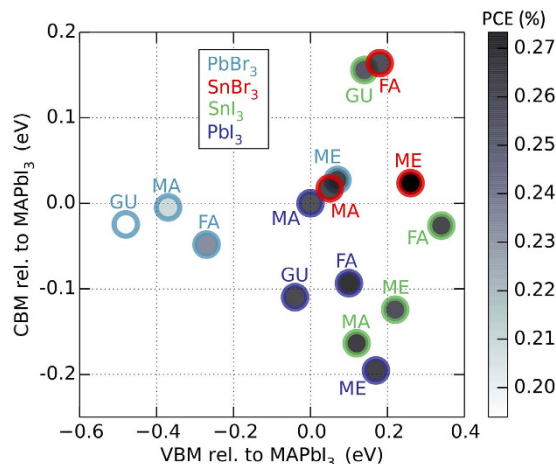


Figure 3. Level alignment in relation to MAPbI₃ in eV. Classes of compounds are colored according to their inorganic backbone: PbI₃ = purple, PbBr₃ = blue, SnI₃ = green, and SnBr₃ = red. The PCE determine the darkness of the fill color in the circles. Note that the spread in VBM is much larger than the spread in CBM. Detailed numerical results are available in the Supplementary Material, Tables 4 and 5.

Methods

First principles calculations. The DFT simulations are performed using the PBE³³ exchange–correlation functional with van der Waals corrections^{34,35}, as implemented in VASP^{36–39}. We also employ the HSE hybrid density functional⁴⁰ for an independent estimate of the relative shifts in band edges. We use a Γ -centered k-point grid of $8 \times 8 \times 8$ and a plane-wave energy cutoff of 550 eV. The SCF loop convergence is halted when the energy difference to previous steps is 10^{-5} eV, structural relaxations are stopped when the energy difference to the previous geometry is 10^{-3} eV. For structural properties integration over the occupied states is performed using Gaussian smearing with a width of 0.1 eV. For core-levels and average potentials the modified tetrahedron method was employed. Further details can be found in the Supplementary Material.

Circuit modelling. The model of the cell is implemented in Python and solved using the NumPy package⁴¹. The graphics is made using matplotlib⁴².

References

- Berry, J. *et al.* Hybrid Organic–Inorganic Perovskites (HOIPs): Opportunities and Challenges. *Adv. Mater.* **27**, 5102–5112 (2015).
- Unger, E. L., Hoke, E. T., Bailie, C. D. & Nguyen, W. H. Hysteresis and transient behavior in current–voltage measurements of hybrid-perovskite absorber solar cells. *Energy Environ. Sci.* **7**, 3690–3698 (2014).
- Wojciechowski, K. *et al.* Heterojunction Modification for Highly Efficient Organic–Inorganic Perovskite Solar Cells. *ACS Nano* **8**, 12701–12709 (2014).
- Stranks, S. D. & Snaith, H. J. Metal-halide perovskites for photovoltaic and light-emitting devices. *Nature Nanotech* **10**, 391–402 (2015).
- Shockley, W. & Queisser, H. J. Detailed Balance Limit of Efficiency of p-n Junction Solar Cells. *J Appl Phys* **32**, 510–511 (1961).
- Meloni, S., Moehl, T., Tress, W. & Frankevičius, M. Ionic polarization-induced current-voltage hysteresis in CH₃NH₃PbX₃ perovskite solar cells. *Nature* **7**, 10334 (2016).
- Sherkar, T. S. & Koster, L. J. A. Can ferroelectric polarization explain the high performance of hybrid halide perovskite solar cells? *Phys. Chem. Chem. Phys.* **18**, 331–338 (2015).
- Bergmann, V. W. *et al.* Real-space observation of unbalanced charge distribution inside a perovskite-sensitized solar cell. *Nature Communications* **5**, 5001 (2014).
- Edri, E. *et al.* Elucidating the charge carrier separation and working mechanism of CH₃NH₃PbI₃-xClx perovskite solar cells. *Nature Communications* **5**, 3461 (2014).
- Marchioro, A. *et al.* Unravelling the mechanism of photoinduced charge transfer processes in lead iodide perovskite solar cells. *Nature Photonics* **8**, 250–255 (2014).
- Motta, C. *et al.* Revealing the role of organic cations in hybrid halide perovskites CH₃NH₃PbI₃. *Nature Communications* **6**, 7026 (2014).
- Kümmel, S. & Kronik, L. Orbital-dependent density functionals: Theory and applications. *Rev Mod Phys* **80**, 3–60 (2008).
- Umari, P., Mosconi, E. & De Angelis, F. Relativistic GW calculations on CH₃NH₃PbI₃ and CH₃NH₃SnI₃ Perovskites for Solar Cell Applications. *Sci. Rep.* **4**, 4467 (2014).
- Filip, M. R. & Giustino, F. GWquasiparticle band gap of the hybrid organic-inorganic perovskite CH₃NH₃PbI₃: Effect of spin-orbit interaction, semicore electrons, and self-consistency. *Phys Rev B* **90**, 245145 (2014).
- Frost, J. M. *et al.* Atomistic Origins of High-Performance in Hybrid Halide Perovskite Solar Cells. *Nano Letters* **14**, 2584–2590 (2014).
- Miyata, A. *et al.* Direct measurement of the exciton binding energy and effective masses for charge carriers in organic–inorganic tri-halide perovskites. *Nature Physics* **11**, 582–587 (2015).
- Galkowski, K., Mitioglu, A. & Miyata, A. Determination of the exciton binding energy and effective masses for methylammonium and formamidinium lead tri-halide perovskite semiconductors. *Energy Environ. Sci.* **9**, 962–970 (2016).
- Dong, Q. *et al.* Electron-hole diffusion lengths > 175 μ m in solution-grown CH₃NH₃PbI₃ single crystals. *Science* **347**, 967–970 (2015).
- Osterloh, F. E. Maximum theoretical efficiency limit of photovoltaic devices: effect of band structure on excited state entropy. *J. Phys. Chem. Lett.* **5**, 3354–3359 (2014).

20. Sha, W. E. I., Ren, X., Chen, L. & Choy, W. C. H. The efficiency limit of CH₃NH₃PbI₃ perovskite solar cells. *Appl Phys Lett* **106**, 221104 (2015).
21. Afanas'ev, V. V. Electron Band Alignment at Interfaces of Semiconductors with Insulating Oxides: An Internal Photoemission Study. *Advances in Condensed Matter Physics* **2014**, 1–30 (2014).
22. Dymshits, A., Henning, A., Segev, G., Rosenwaks, Y. & Etgar, L. The electronic structure of metal oxide/organo metal halide perovskite junctions in perovskite based solar cells. *Sci. Rep.* **5**, 8704 (2015).
23. Jiang, C.-S. *et al.* Carrier separation and transport in perovskite solar cells studied by nanometre-scale profiling of electrical potential. *Nature Communications* **6**, 8397 (2015).
24. Van de Walle, C. G. Band lineups and deformation potentials in the model-solid theory. *Phys Rev B* **39**, 1871–1883 (1989).
25. Franciosi, A. & Van de Walle, C. G. Heterojunction band offset engineering. *Surface Science Reports* **25**, 1–140 (1996).
26. Massidda, S., Min, B. I. & Freeman, A. J. Interface phenomena at semiconductor heterojunctions: Local-density valence-band offset in GaAs/AlAs. *Phys Rev B* **35**, 9871–9874 (1987).
27. Wei, S.-H. & Zunger, A. Calculated natural band offsets of all II {endash} VI and III {endash} V semiconductors: Chemical trends and the role of cation {ital d} orbitals. *Appl Phys Lett* **72**, 2011 (1998).
28. Lang, L. *et al.* Three-step approach for computing band offsets and its application to inorganic ABX₃halide perovskites. *Phys Rev B* **92**, 075102 (2015).
29. Butler, K. T., Kumagai, Y., Oba, F. & Walsh, A. Screening procedure for structurally and electronically matched contact layers for high-performance solar cells: hybrid perovskites. *Journal of Materials Chemistry C* **4**, 1149–1158 (2016).
30. Mosconi, E., Umari, P. & De Angelis, F. Electronic and optical properties of mixed Sn–Pb organohalide perovskites: a first principles investigation. *J. Mater. Chem. A* **3**, 9208–9215 (2015).
31. Lang, L., Yang, J.-H., Liu, H.-R., Xiang, H. J. & Gong, X. G. First-principles study on the electronic and optical properties of cubic ABX₃ halide perovskites. *Phys Lett A* **378**, 290–293 (2014).
32. Butler, K. T., Frost, J. M. & Walsh, A. Band alignment of the hybrid halide perovskites CH₃NH₃PbCl₃, CH₃NH₃PbBr₃ and CH₃NH₃PbI₃. *Materials Horizons* **2**, 228–231 (2015).
33. Perdew, J. P. Generalized gradient approximation made simple. *Phys Rev Lett* **77**, 3865–3868 (1996).
34. Tkatchenko, A. & Scheffler, M. Accurate Molecular Van Der Waals Interactions from Ground-State Electron Density and Free-Atom Reference Data. **102**, 073005 (2009).
35. Bučko, T., Lebegue, S., Hafner, J. & Ángyán, J. G. Improved Density Dependent Correction for the Description of London Dispersion Forces. *J Chem Theory Comput* **9**, 4293–4299 (2013).
36. Kresse, G. & Hafner, J. Ab initio molecular dynamics for liquid metals. *Phys Rev B* **47**, 558–561 (1993).
37. Kresse, G. & Hafner, J. Ab initio molecular-dynamics simulation of the liquid-metal–amorphous-semiconductor transition in germanium. *Phys Rev B* **14251–14269** (1994).
38. Kresse, G. Efficiency of ab-initio total energy calculations for metals and semiconductors using a plane-wave basis set. *Comp Mat Sci* **6**, 15–50 (1996).
39. Kresse, G. & Joubert, D. From ultrasoft pseudopotentials to the projector augmented-wave method. *Phys Rev B* **59**, 1758–1775 (1999).
40. Heyd, J., Scuseria, G. E. & Ernzerhof, M. Erratum: ‘Hybrid functionals based on a screened Coulomb potential’ [*J. Chem. Phys.* **118**, 8207 (2003)]. *J. Chem. Phys.* **124**, 219906 (2006).
41. van der Walt, S., Colbert, S. C. & Varoquaux, G. The NumPy Array: A Structure for Efficient Numerical Computation. *Comput Sci Eng* **13**, 22–30 (2011).
42. Hunter, J. D. Matplotlib: A 2D Graphics Environment. *Comput Sci Eng* **9**, 90–95 (2007).

Acknowledgements

The work of O.G. was supported by the Swedish Research Council (VR) Grant No. 637–2013–7303 and the Ingegerd Bergh foundation. D.V. was supported by National Science Foundation Catalysis program under Grant No. CHE-1362616. Computational resources were provided by NSC under the allocation SNIC 2014-1-343 and by XSEDE (Grant No. TG-DMR120073), which is supported by National Science Foundation Grant No. ACI-1053575. G. Kolesov, C. Flamant and M. Montemore are acknowledged for their insightful comments.

Author Contributions

O.G. and D.V. carried out the first principles calculations. O.G. carried out the implementation of the efficiency modeling. All authors analyzed and discussed the results. All authors contributed to writing the manuscript. E.K. supervised the project.

Additional Information

Supplementary information accompanies this paper at <http://www.nature.com/srep>

Competing financial interests: The authors declare no competing financial interests.

How to cite this article: Grånäs, O. *et al.* Establishing the limits of efficiency of perovskite solar cells from first principles modeling. *Sci. Rep.* **6**, 36108; doi: 10.1038/srep36108 (2016).

Publisher's note: Springer Nature remains neutral with regard to jurisdictional claims in published maps and institutional affiliations.



This work is licensed under a Creative Commons Attribution 4.0 International License. The images or other third party material in this article are included in the article's Creative Commons license, unless indicated otherwise in the credit line; if the material is not included under the Creative Commons license, users will need to obtain permission from the license holder to reproduce the material. To view a copy of this license, visit <http://creativecommons.org/licenses/by/4.0/>

© The Author(s) 2016